

LiMn₂O_{4-y}Br_y Nanoparticles Synthesized by a Room Temperature Solid-State Coordination Method

Yudai Huang · Rongrong Jiang · Shu-Juan Bao ·
Yali Cao · Dianzeng Jia

Received: 22 July 2008 / Accepted: 8 January 2009 / Published online: 22 January 2009
© to the authors 2009

Abstract LiMn₂O_{4-y}Br_y nanoparticles were synthesized successfully for the first time by a room temperature solid-state coordination method. X-ray diffractometry patterns indicated that the LiMn₂O_{4-y}Br_y powders were well-crystallized pure spinel phase. Transmission electron microscopy images showed that the LiMn₂O_{4-y}Br_y powders consisted of small and uniform nanosized particles. Synthesis conditions such as the calcination temperature and the content of Br⁻ were investigated to optimize the ideal condition for preparing LiMn₂O_{4-y}Br_y with the best electrochemical performances. The optimized synthesis condition was found in this work; the calcination temperature is 800 °C and the content of Br⁻ is 0.05. The initial discharge capacity of LiMn₂O_{3.95}Br_{0.05} obtained from the optimized synthesis condition was 134 mAh/g, which is far higher than that of pure LiMn₂O₄, indicating introduction of Br⁻ in LiMn₂O₄ is quite effective in improving the initial discharge capacity.

Keywords LiMn₂O_{4-y}Br_y · Nanoparticles · Room temperature solid-state coordination method · Lithium-ion battery

Introduction

Development of the cathode materials for lithium-ion battery is vital to meet the demands of portable devices, power tools, e-bikes, future usages of electric vehicles, and so on [1]. Among three promising candidates for cathode materials (LiCoO₂, LiNiO₂, and LiMn₂O₄), lithium manganese oxides (LiMn₂O₄) [2] are inexpensive cathode materials with a high energy density, environmental acceptability, and are more abundant in nature. In spite of these advantages, LiMn₂O₄ has the problem of severe capacity fading during charge and discharge cycles [3, 4], which makes it unsuitable for commercial application. Intensive research has particularly focused on the mechanism of capacity fading and has suggested numerous solutions.

Among these projects, doping [5, 6] is considered to be an effective path to improve the electrochemical performance of spinel LiMn₂O₄, so several attempts have been made for improving the lithium manganese spinels by doping various metals ions [7–10]. Although such substitutions often result in enhancing the stability of spinel, the first discharge capacity of them is considerably lower than that of the parent compound. The reduction in the first discharge capacity is mainly due to the fact that the substituent ions do not contribute to the discharge capacity. In 1999, Amatucci et al. [11] and Palacin et al. [12] reported that the introduction of the anion in spinel structure can reduce the Mn oxidation state and then increase the first discharge capacity. These interesting results derived from the anion doping stimulated our research interest to investigate the effect of other anions doping. To the best of our knowledge, up to now, no Br⁻-doped cathode materials (LiMn₂O_{4-y}Br_y) have been reported.

It is believed that single-phase, homogeneity, uniform particle morphology with nanometer size distribution is the

Y. Huang · R. Jiang · S.-J. Bao · Y. Cao · D. Jia (✉)
Institute of Applied Chemistry, Xinjiang University,
Urumqi 830046, People's Republic of China
e-mail: jdz@xju.edu.cn

Y. Huang · Y. Cao · D. Jia
School of Science, Xi'an Jiaotong University,
Xi'an 710049, People's Republic of China

desired feature for achieving a higher electrode activity [13]. Nanometer-scale structured electrode materials are of great interest as potential building blocks for future generation electronic devices with greatly reduced size [14], because they show higher capacity and better cycling performance than conventional electrodes composed of this kind of materials [15]. There have been increased interests in synthesizing nanostructures and their derivative compounds for their diverse physicochemical properties and potential applications as cathode materials for lithium-ion batteries [16]. Moreover, it is well known that the preparation methods and post-treatment techniques could influence the structure and electrochemical performance of materials significantly [17–19]. Further, the subtle variation of chemical composition [20, 21] will bring great changes in the electrochemical performance of products. Room temperature solid-state coordination method [22, 23] possesses the advantages of simple manipulation and better prospects for commercialization as compared to the conventional solid-state method [24]. More meaningfully, it achieves homogeneous mixture of the starting components, a low synthesis temperature and small grain size of the powders. Besides this, several nanomaterials have been synthesized using this method [25–27]. In this study, $\text{LiMn}_2\text{O}_{4-y}\text{Br}_y$ nanoparticles were synthesized successfully for the first time by a room temperature solid-state coordination method. The structures, morphologies, and electrochemical properties of these materials were also investigated.

Experimental

Stoichiometric lithium acetate, manganese acetate, lithium bromide, and citric acid (worked as chelating reagent, molar ratio of citric acid to the total metal ions is 1:1), which were ground into powders separately, were mixed with polyethylene glycol (PEG) 400 (worked as dispersants) in an agate mortar and ground with a pestle for 1.5 h in order to make them react to reach the best possible homogeneity. Then the mixtures were dried at 120 °C for 8 h to form precursors. The obtained precursors were annealed at 500 °C for 1 h, after ground, held at 600–800 °C for 10 h in air in a muffle furnace to obtain final $\text{LiMn}_2\text{O}_{4-y}\text{Br}_y$ powders. Figure 1 shows the flowchart.

An X-ray diffractometer (XRD) (MXP18AHF, Mac, Japan) with Cu K α radiation ($\lambda = 1.54056 \text{ \AA}$) was used for the identification of the crystalline phases of the powders. The morphological characteristics of the products were investigated using transmission electron microscope (TEM, H-600, Hitachi, Japan).

The cells consisted of a LiMn_2O_4 -based composite as the positive electrode, a Li disk as the negative electrode,

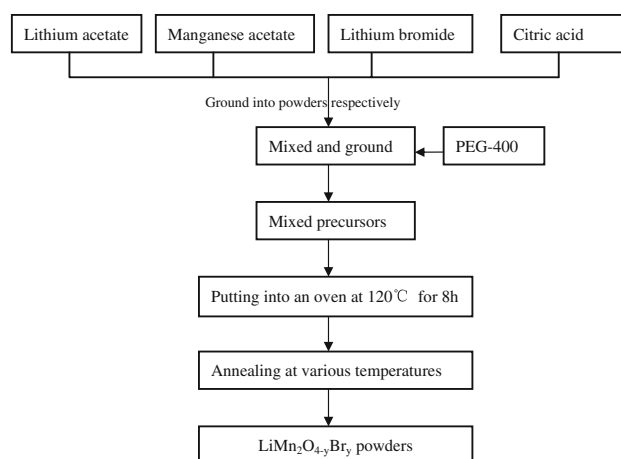


Fig. 1 Flowchart showing the synthesis of $\text{LiMn}_2\text{O}_{4-y}\text{Br}_y$ samples by room temperature solid-state coordination method

and an electrolyte of 1 M LiPF_6 in a 1:1 (volume ratio) mixture of ethylene carbonate (EC)/dimethyl carbonate (DMC). The cathode was formed by mixing the active material with acetylene black and PVDF binder in 85:10:5 ratio in *N*-methyl-pyrrolidone (NMP). NMP acts as the solvent for the binder. The paste was applied to an aluminum foil current collector using a blade. The film was dried at 60 °C in air for 1 h and then was vacuum dried at 120 °C for 4 h. Celgard 2300 membrane was used as the separator. The cells were assembled in an argon-filled glove box. All the electrochemical tests were carried out at room temperature. Cyclic voltammetry (CV) (CHI660B Electrochemical Workstation Chenhua Co. of Shanghai, China) experiments were conducted from 3.2 to 4.35 V at a scan rate of 0.1 mV/s, and a Li metal disk served as both counter and reference electrode. Charge/discharge tests were performed at a constant current density of 0.30 mA/cm² within the potential range of 3.0 and 4.35 V.

Results and Discussion

The XRD patterns of $\text{LiMn}_2\text{O}_{4-y}\text{Br}_y$ powders calcinated at 600–800 °C for 10 h are shown in Fig. 2. The XRD of the powders calcinated at 600 °C shows the impurity peaks of Mn_2O_3 (marked by ▼). The formation of impurity phase Mn_2O_3 indicates that the temperature is not high enough to reach full crystallization and containing some vacancies in LiMn_2O_4 structure during combustion. When the calcination temperature increases to 700 °C, the impurity peaks of Mn_2O_3 disappear and the pure spinel LiMn_2O_4 structure forms, which indicates that pure spinel LiMn_2O_4 can be produced by heat treatment at relatively higher temperatures. Moreover, when the temperature increases, the intensity of peaks grows correspondingly, which indicates better crystallization is obtained. The diffraction peaks of

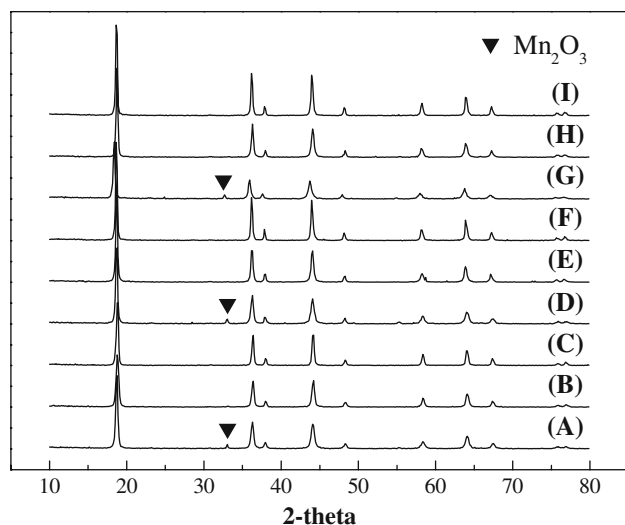


Fig. 2 XRD patterns of $\text{LiMn}_2\text{O}_{4-y}\text{Br}_y$: (A) LiMn_2O_4 calcinated at 600 °C; (B) LiMn_2O_4 calcinated at 700 °C; (C) LiMn_2O_4 calcinated at 800 °C; (D) $\text{LiMn}_2\text{O}_{3.95}\text{Br}_{0.05}$ calcinated at 600 °C; (E) $\text{LiMn}_2\text{O}_{3.95}\text{Br}_{0.05}$ calcinated at 700 °C; (F) $\text{LiMn}_2\text{O}_{3.95}\text{Br}_{0.05}$ calcinated at 800 °C; (G) $\text{LiMn}_2\text{O}_{3.90}\text{Br}_{0.10}$ calcinated at 600 °C; (H) $\text{LiMn}_2\text{O}_{3.90}\text{Br}_{0.10}$ calcinated at 700 °C; (I) $\text{LiMn}_2\text{O}_{3.90}\text{Br}_{0.10}$ calcinated at 800 °C

$\text{LiMn}_2\text{O}_{3.95}\text{Br}_{0.05}$ and $\text{LiMn}_2\text{O}_{3.90}\text{Br}_{0.10}$ synthesized at 700 and 800 °C corresponded to pure phase spinel structure. The results indicate that the structure of the ternary spinel remains when some of the O^{2-} in the spinel phase are replaced by Br^- . Doping do not seem to change the spinel structure of the samples because no other impurity peaks are observed in the XRD patterns. The lattice constants of all the samples, which are calculated from the XRD spectra, are summarized in Table 1. The samples with the same chemical compositions calcined at different temperatures have little difference in lattice constants. However, the products doped with Br^- have larger lattice constants, which is ascribed to the substitution of O^{2-} by Br^- . The Br^- has larger ion (1.96 Å) radius than that of O^{2-} (1.4 Å)

Table 1 Lattice constants calculated from the XRD spectra

Nominal composition	Calcination temperature (°C)	Lattice parameter (a/nm)
LiMn_2O_4	600	0.8215
	700	0.8213
	800	0.8210
$\text{LiMn}_2\text{O}_{3.95}\text{Br}_{0.05}$	600	0.8223
	700	0.8221
	800	0.8220
$\text{LiMn}_2\text{O}_{3.90}\text{Br}_{0.10}$	600	0.8233
	700	0.8229
	800	0.8226

and Br^- substitution leads to reduction of Mn^{4+} to the larger Mn^{3+} cations, which results in improving capacity as reported by Amatucci et al. [21]. Because the powders calcinated at 600 °C show the impurity peaks of Mn_2O_3 , we did not do the electrochemistry test of them.

The trend of morphology variation of different $\text{LiMn}_2\text{O}_{4-y}\text{Br}_y$ with temperature is similar, so the TEM of $\text{LiMn}_2\text{O}_{3.95}\text{Br}_{0.05}$ powders calcinated at 600–800 °C for 10 h are given as examples in Fig. 3. The sample calcined at 600 °C agglomerates severely and its size is about 200 nm. This maybe due to some Mn_2O_3 impurity existing in the sample. As the temperature increases to 700 °C, the distribution of the particle size becomes narrow and the average particle size is about 100 nm. The decrease of particle size is due to the breaking of agglomerated powders as the calcination temperature increases, but agglomeration still exists. As the temperature increases further, it presents the spherical particle morphology, homogenous particle composition and narrow distribution of particle size. The extent of agglomeration of particles in the sample is meliorated. The particle size of the sample calcined at 600 °C is larger than that of the sample calcined at 700 and 800 °C, which indicates the calcination temperature has significant effect on the crystallization and morphology of the samples. This agreed well with the result of XRD. Products with nanosized particles would facilitate reducing the diffusion length of the lithium ions during intercalation and deintercalation processes, which would improve the electrochemical performance of the samples [28].

Cyclic voltammograms of the $\text{Li}/\text{LiMn}_2\text{O}_{4-y}\text{Br}_y$ cells between 3.2 and 4.35 V at a scan rate of 0.1 mV/s for the first cycle are shown in Fig. 4. The cyclic voltammograms reveal that there are two pairs of redox peaks on each cycle voltammograms. The two pairs of redox peaks correspond to two-step reversible intercalation/deintercalation reaction. The samples synthesized at 800 °C present higher current peaks than the ones prepared at 700 °C. The $\text{LiMn}_2\text{O}_{3.95}\text{Br}_{0.05}$ samples synthesized at 800 °C possess the highest current peaks, which indicates that the product calcined at 800 °C might have better electrochemical activity.

Figure 5 displays voltage versus discharge capacity curves for $\text{LiMn}_2\text{O}_{4-y}\text{Br}_y$ between 3 and 4.35 V versus $\text{Li}/\text{LiMn}_2\text{O}_{4-y}\text{Br}_y$ by applying 0.3 mA/cm² at room temperature. For $\text{LiMn}_2\text{O}_{4-y}\text{Br}_y$ sample prepared at 700 °C, the initial discharge capacity of pure spinel is 106 mAh/g. It increases to 127 mAh/g as $y = 0.05$ and decreases to 118 mAh/g as $y = 0.10$. It is clear that the increase of initial discharge capacity results from Br^- doping. This may be explained by the following reasons. The substitution of monovalent Br^- for divalent O^{2-} results in the increasing of Mn^{3+} content in spinel which contributes to

Fig. 3 TEM photographs of $\text{LiMn}_2\text{O}_{3.95}\text{Br}_{0.05}$: (a) calcinated at 600 °C, (b) 700 °C, and (c) 800 °C

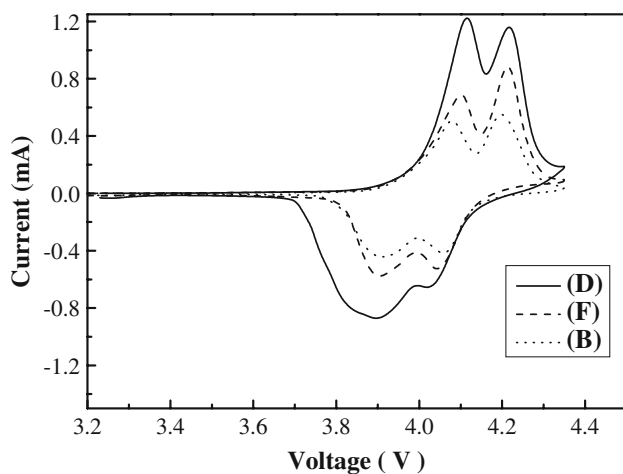
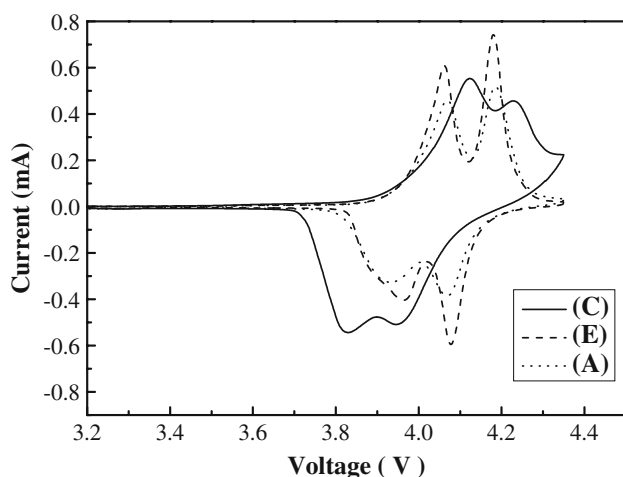
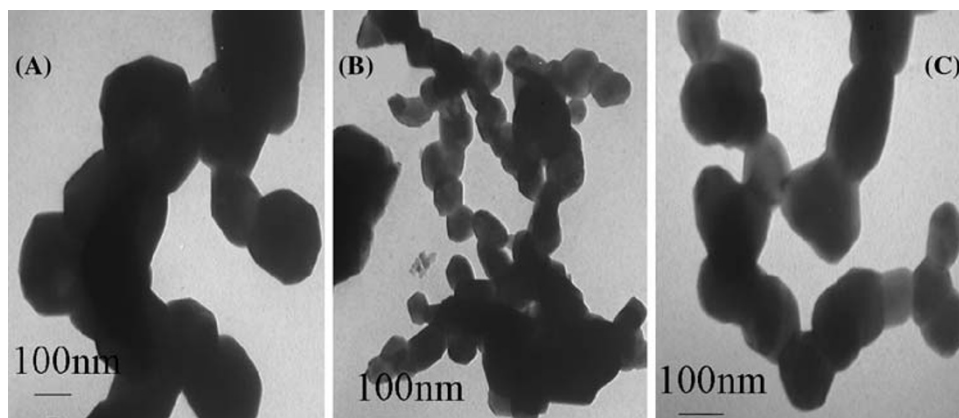


Fig. 4 Cyclic voltammogram of $\text{Li}/\text{LiMn}_2\text{O}_{4-y}\text{Br}_y$ cells between 3.2 and 4.35 V at scan rate of 0.1 mV/s: (A) LiMn_2O_4 calcinated at 700 °C; (B) LiMn_2O_4 calcinated at 800 °C; (C) $\text{LiMn}_2\text{O}_{3.95}\text{Br}_{0.05}$ calcinated at 700 °C; (D) $\text{LiMn}_2\text{O}_{3.95}\text{Br}_{0.05}$ calcinated at 800 °C; (E) $\text{LiMn}_2\text{O}_{3.90}\text{Br}_{0.10}$ calcinated at 700 °C; (F) $\text{LiMn}_2\text{O}_{3.90}\text{Br}_{0.10}$ calcinated at 800 °C

charge/discharge capacity during intercalation/deintercalation of Li^+ in LiMn_2O_4 . Moreover, Br^- doping brings in larger lattice constants of samples, thus Li^+ can move more

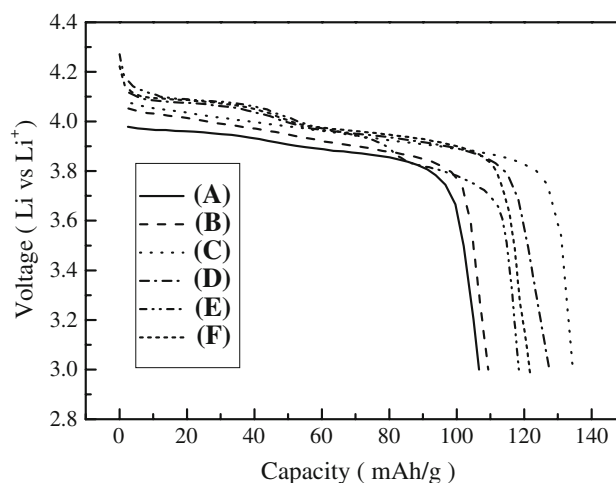


Fig. 5 Voltage versus discharge capacity curves of $\text{LiMn}_2\text{O}_{4-y}\text{Br}_y$: (A) LiMn_2O_4 calcinated at 700 °C; (B) LiMn_2O_4 calcinated at 800 °C; (C) $\text{LiMn}_2\text{O}_{3.95}\text{Br}_{0.05}$ calcinated at 800 °C; (D) $\text{LiMn}_2\text{O}_{3.95}\text{Br}_{0.05}$ calcinated at 700 °C; (E) $\text{LiMn}_2\text{O}_{3.90}\text{Br}_{0.10}$ calcinated at 700 °C; (F) $\text{LiMn}_2\text{O}_{3.90}\text{Br}_{0.10}$ calcinated at 800 °C

freely in the sample and this might help increase the capacity [21]. When the calcination temperature increases to 800 °C, $\text{LiMn}_2\text{O}_{4-y}\text{Br}_y$ samples deliver initial discharge capacity of 109, 134, and 121 mAh/g as $y = 0, 0.05$, and 0.10, respectively. Samples calcined at relatively higher temperature have higher initial discharge capacity. The $\text{LiMn}_2\text{O}_{3.95}\text{Br}_{0.05}$ synthesized at 800 °C possess the highest initial discharge capacity. However, with the increase of Br^- content in spinel (from 0.05 to 0.10), the initial discharge capacity decreases, which maybe due to Br^- doping that can improve the initial discharge capacity, but the Br^- content has an optimal value. In this work, the optimal value is 0.05.

The above-mentioned results show that effective anion doping can result in improvement of initial discharge capacity. Figure 6 displays the variations of discharge capacity versus cycle number curves of $\text{LiMn}_2\text{O}_{4-y}\text{Br}_y$ between 3 and 4.35 V versus $\text{Li}/\text{LiMn}_2\text{O}_{4-y}\text{Br}_y$ by applying 0.3 mA/cm² at room temperature. As can be seen from

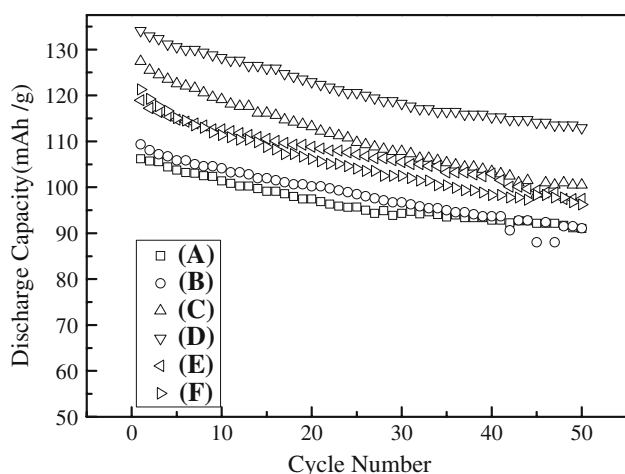


Fig. 6 Discharge capacity versus cycle number curves of $\text{LiMn}_2\text{O}_{4-y}\text{Br}_y$: (A) LiMn_2O_4 calcinated at 700°C ; (B) LiMn_2O_4 calcinated at 800°C ; (C) $\text{LiMn}_2\text{O}_{3.95}\text{Br}_{0.05}$ calcinated at 700°C ; (D) $\text{LiMn}_2\text{O}_{3.95}\text{Br}_{0.05}$ calcinated at 800°C ; (E) $\text{LiMn}_2\text{O}_{3.90}\text{Br}_{0.10}$ calcinated at 700°C ; (F) $\text{LiMn}_2\text{O}_{3.90}\text{Br}_{0.10}$ calcinated at 800°C

Fig. 6, the samples doped by Br^- have larger initial discharge capacity than the pure spinels. However, Br^- -doped samples present appreciably high capacity loss than the parent compound. For $\text{LiMn}_2\text{O}_{4-y}\text{Br}_y$ sample prepared at 700°C , the capacity retention rate of pure spinel is 86%. It decreases to 79% as $y = 0.05$ and 82% as $y = 0.10$. For $\text{LiMn}_2\text{O}_{4-y}\text{Br}_y$ sample prepared at 800°C , the capacity retention rate of pure spinel is 83%. It decreases to 82% as $y = 0.05$ and 79% as $y = 0.10$. The $\text{LiMn}_2\text{O}_{4-y}\text{Br}_y$ ($y = 0.05, 0.10$) samples have higher initial discharge capacity but lower cycle life than that of the parent compound. This is due to the increase of Mn^{3+} content by monovalent Br^- substitution for divalent O^{2-} . The high-spin Mn^{3+} ions give rise to the Jahn-Teller distortion which is the origin of the capacity loss. In a word, the increase of Mn^{3+} causes two effects: (1) the increase of initial discharge capacity and (2) the decrease of the capacity retention. As reported by many literatures, surface modification and cation codoping can overcome Jahn-Teller distortion [29]. Sun et al. [30, 31] reported that $\text{LiAl}_{0.34}\text{Mn}_{1.76}\text{O}_{3.98}\text{S}_{0.02}$ and $\text{Li}_{1.03}\text{Al}_{0.2}\text{Mn}_{1.8}\text{O}_{3.96}\text{S}_{0.04}$ materials prepared via a sol-gel method showed excellent cyclability in both 4 and 3 V regions. In our lab, the research work of Br^- and Al^{3+} codoping for improvement of the electrochemical performance of spinel LiMn_2O_4 is undergoing.

Conclusion

In this work, $\text{LiMn}_2\text{O}_{4-y}\text{Br}_y$ nanoparticles were synthesized by a room temperature solid-state coordination method for the first time. The powders have homogeneous morphology, small particles, and high crystallinity. The

CV and charge/discharge test revealed that Br^- doping improves the initial discharge capacity of the samples. The $\text{LiMn}_2\text{O}_{3.95}\text{Br}_{0.05}$ calcinated at 800°C has an initial discharge capacity of 134 mAh/g.

Acknowledgments This work was partially supported by the Nature Science Foundation of Xinjiang Province (grant nos. 200821121 and 200721102) and the National Nature Science Foundation of China (grant nos. 20666005 and 20661003).

References

- J.M. Tarascon, M. Armand, *Nature* **414**, 35 (2001). doi:10.1038/35104644
- J.M. Tarascon, E. Wang, F.K. Shokoohi, W.R. McKinnon, S. Colson, *J. Electrochem. Soc.* **138**, 2859 (1991). doi:10.1149/1.2085330
- R.J. Gummow, A. de Kock, M.M. Thackeray, *Solid State Ionics* **69**, 59 (1994). doi:10.1016/0167-2738(94)90450-2
- Y. Xia, Y. Zhou, M. Yoshio, *J. Electrochem. Soc.* **144**, 2593 (1997). doi:10.1149/1.1837870
- Y.P. Wu, E. Rahm, R. Holze, *Electrochim. Acta* **47**, 3491 (2002). doi:10.1016/S0013-4686(02)00317-1
- G. Amatucci, A.D. Pasquier, A. Blyr, T. Zheng, J.M. Tarascon, *Electrochim. Acta* **45**, 255 (1999). doi:10.1016/S0013-4686(99)00209-1
- S. Komaba, K. Oikawa, S.T. Myung, N. Kumagai, T. Kamiyama, *Solid State Ionics* **149**, 47 (2002). doi:10.1016/S0167-2738(02)00168-6
- Y.D. Huang, J. Li, D.Z. Jia, *J. Colloid Interface Sci.* **286**, 263 (2005)
- M. Yoshio, Y. Xia, N. Kumada, S. Ma, *J. Power Sources* **101**, 79 (2001). doi:10.1016/S0378-7753(01)00546-8
- J.H. Lee, J.K. Hong, D.H. Jang, Y.K. Sun, S.M. Oh, *J. Power Sources* **89**, 7 (2000). doi:10.1016/S0378-7753(00)00375-X
- G.G. Amatucci, N. Pereira, T. Zhang, I. Plitz, J.M. Tarascon, *J. Power Sources* **81–82**, 39 (1999). doi:10.1016/S0378-7753(99)00186-X
- M.R. Palacin, F.L. Cras, L. Seguin, M. Anne, Y. Chabre, J.M. Tarascon, G. Amatucci, G. Vaughan, P. Strobel, *J. Solid State Chem.* **144**, 361 (1999). doi:10.1006/jssc.1999.8166
- C.Z. Lu, G.T.K. Fey, *J. Phys. Chem. Solids* **67**, 756 (2006). doi:10.1016/j.jpcs.2005.11.008
- H. Dai, E.W. Wong, C.M. Libeber, *Science* **272**, 523 (1996). doi:10.1126/science.272.5261.523
- Y.K. Zhou, C.M. Shen, H.L. Li, *Solid State Ionics* **146**, 81 (2002). doi:10.1016/S0167-2738(01)01005-0
- A. Doble, K. Ngala, S. Yang, P.Y. Zavalij, M.S. Whittingham, *Chem. Mater.* **13**, 4382 (2001). doi:10.1021/cm010518h
- Y.K. Sun, C.S. Yoon, C.K. Kim, S.G. Youn, Y.S. Lee, M. Yoshio, I.H. Oh, *J. Mater. Chem.* **11**, 2519 (2001). doi:10.1039/b103709a
- P. Barboux, J.M. Tarascon, F.K. Shokoohi, *J. Solid State Chem.* **94**, 185 (1991). doi:10.1016/0022-4596(91)90231-6
- G.X. Wang, D.H. Bradhurst, H.K. Liu, S.X. Dou, *Solid State Ionics* **120**, 95 (1999). doi:10.1016/S0167-2738(98)00554-2
- P. Endres, B. Fuchs, S. Kemmler-Sack, K. Brandt, G. Faust-Becker, H.-W. Praas, *Solid State Ionics* **89**, 221 (1996)
- G. Amatucci, J.M. Tarascon, *J. Electrochem. Soc.* **149**, K31 (2002). doi:10.1149/1.1516778
- X.R. Ye, D.Z. Jia, J.Q. Yu, X.Q. Xin, Z.L. Xue, *Adv. Mater.* **11**, 941 (1999). doi:10.1002/(SICI)1521-4095(199908)11:11<941::AID-ADMA941>3.0.CO;2-T

23. R.Y. Wang, D.Z. Jia, L. Zhang, L. Liu, Z.P. Guo, B.Q. Li, J.X. Wang, *Adv. Funct. Mater.* **16**, 687 (2006). doi:[10.1002/adfm.200500549](https://doi.org/10.1002/adfm.200500549)
24. H.M. Wu, J.P. Tu, Y.F. Yuan, Y. Li, X.B. Zhao, G.S. Gao, *Mater. Chem. Phys.* **93**, 461 (2005). doi:[10.1016/j.matchemphys.2005.03.036](https://doi.org/10.1016/j.matchemphys.2005.03.036)
25. D.Z. Jia, J.Q. Yu, X. Xia, *Chin. Sci. Bull.* **43**, 571 (1998). doi:[10.1007/BF02883641](https://doi.org/10.1007/BF02883641)
26. T.Y. Zhou, X.Q. Xin, *Nanotechnology* **15**, 534 (2004). doi:[10.1088/0957-4484/15/5/022](https://doi.org/10.1088/0957-4484/15/5/022)
27. Z.P. Sun, L. Liu, L. Zhang, D.Z. Jia, *Nanotechnology* **17**, 2266 (2006). doi:[10.1088/0957-4484/17/9/032](https://doi.org/10.1088/0957-4484/17/9/032)
28. Y.K. Zhou, H.L. Li, *J. Mater. Chem.* **12**, 681 (2002). doi:[10.1039/b107718j](https://doi.org/10.1039/b107718j)
29. D. Capsoni, M. Bini, G. Chiodelli, P. Mustarelli, V. Massarotti, C.B. Azzoni, M.C. Mozzati, L. Linati, *J. Phys. Chem. B* **106**, 7432 (2002). doi:[10.1021/jp020220u](https://doi.org/10.1021/jp020220u)
30. Y.K. Sun, Y.S. Jeon, *J. Mater. Chem.* **9**, 3147 (1999). doi:[10.1039/a906811b](https://doi.org/10.1039/a906811b)
31. Y.K. Sun, *Electrochem. Commun.* **2**, 6 (2000)